

Epitaxy of Nanocrystalline Silicon Carbide on Si(111) at Room Temperature

Roberto Verucchi,^{*,†} Lucrezia Aversa,[†] Marco V. Nardi,^{†,◆} Simone Taioli,^{*,‡,§,||} Silvio a Beccara,^{‡,§} Dario Alfè,^{‡,¶,∇} Lucia Nasi,[○] Francesca Rossi,[○] Giancarlo Salviati,[○] and Salvatore Iannotta[○]

[†]Istituto dei Materiali per l'Elettronica ed il Magnetismo, IMEM-CNR, Sezione FBK di Trento, 38123 Trento, Italy

[‡]Interdisciplinary Laboratory for Computational Science, FBK-CMM and University of Trento, 38123 Trento, Italy

[§]Department of Physics, University of Trento, 38123 Trento, Italy, and Istituto Nazionale di Fisica Nucleare, Sezione di Perugia, 06123 Perugia, Italy

^{||}Dipartimento di Chimica, Università di Bologna, 40126 Bologna, Italy

[∇]Department of Earth Sciences, [¶]Department of Physics and Astronomy, and [○]London Centre for Nanotechnology, University College London, Gower Street, London WC1E 6BT, U.K.

[○]Istituto dei Materiali per l'Elettronica ed il Magnetismo, IMEM-CNR, Parco Area delle Scienze 37/A, 43124 Parma, Italy

Supporting Information

ABSTRACT: Silicon carbide (SiC) has unique chemical, physical, and mechanical properties. A factor strongly limiting SiC-based technologies is the high-temperature synthesis. In this work, we provide unprecedented experimental and theoretical evidence of 3C-SiC epitaxy on silicon at room temperature by using a buckminsterfullerene (C_{60}) supersonic beam. Chemical processes, such as C_{60} rupture, are activated at a precursor kinetic energy of 30–35 eV, far from thermodynamic equilibrium. This result paves the way for SiC synthesis on polymers or plastics that cannot withstand high temperatures.

Silicon carbide (SiC) has unique properties that make it suitable for hard and protective coatings, optoelectronics, and sensing.¹ It is the most promising alternative to Si for electronics devices working at high power/high frequency or under prohibitive conditions.² A new perspective is now being pursued for SiC as a material for biomedical applications.³ As the substrate for the synthesis of high-quality graphene, SiC is expected to be one the most promising interface for graphene-based electronics.⁴

Despite the use of different growth approaches, the synthesis of high-quality/low-defect SiC crystalline films still represents an open challenge.^{2,5} In particular, SiC epitaxy on Si is interesting for the synthesis of the cubic (3C) polytype of SiC, which potentially has the best electrical properties.¹ In this case, molecular beam epitaxy (MBE) has been demonstrated as a viable approach to 3C-SiC/Si synthesis at ~ 1200 K, using buckminsterfullerene (C_{60}) as the C precursor.^{6–10} The epitaxy is critically affected by three factors: high lattice/thermal mismatches between SiC and Si, the high material processing temperature ($T \geq 1100$ K), and Si diffusion through the SiC film, creating defects at the nano- and microscale.⁵ Therefore, synthesizing SiC at lower T is highly desirable to reduce side-growth processes, film defectivity, and production costs.

In this work, we accomplished the room-temperature (RT = 300 K) synthesis of nanocrystalline 3C-SiC on the Si(111) 7×7

surface using the supersonic MBE (SuMBE) approach. In these experiments, the C_{60} translational kinetic energy (KE) reaches values of 30–35 eV by aerodynamic acceleration in vacuum,^{11–14} activating chemical processes on the Si surface. Furthermore, we simulated the C_{60} -Si(111) 7×7 collision using density functional theory (DFT) and found that to obtain cage rupture at the observed kinetic energies, one needs to go beyond the Born–Oppenheimer (BO) approximation and use nonadiabatic molecular dynamics (NA-MD) to intertwine the electronic and nuclear motions.

Submonolayer (sub-ML) C_{60} films were deposited with two different precursor KEs of 30 eV (0.30 ML, 0.65 ML) and 35 eV (0.35 ML, 0.70 ML). The chemical/physical properties of the C_{60} films were investigated by in situ X-ray (XPS) and ultraviolet (UPS) photoelectron spectroscopies. Details can be found in the Supporting Information (SI). The C 1s core level (CL) analysis revealed different characteristics for the 35 eV (Figure 1a,b) and 30 eV (Figure 1c,d) films, but all of the peaks could be well-reproduced by the same four components, labeled P1, P2, P3, and P4. P1 is located at a binding energy (BE) of 283.03 eV and represents photoemission of C in SiC, amorphous/stoichiometric carbide^{7,15} and 3C-SiC.¹⁶ P2 (BE = 283.73 eV) is associated with nonstoichiometric SiC compounds¹⁷ or hexagonal SiC polytypes.¹⁸ P3 (BE = 284.46 eV) and P4 (BE = 285.10 eV) are related to formation of few covalent bonds by C_{60} ^{6–10,13–15} or weak C_{60} -Si interactions. P1 and P2 have been observed only in experiments involving C_{60} on Si at $T \geq 1000$ K; P3 has been observed at $T = 700$ K, while P4 is typical of physisorbed cages. As shown in Figure 1e, at a C_{60} KE of 35 eV, the reacted-species peak areas (P1 and P2) represented >50% of the total C 1s CL for both films, with P2 always being the most intense peak. In contrast, at a C_{60} KE of 30 eV, the weight of the reacted species decreased in going from 0.30 to 0.65 ML, with P4 becoming the most intense. In terms of absolute intensity, at the higher coverage all of the peaks showed a significant increase at

Received: August 6, 2012

Published: October 11, 2012

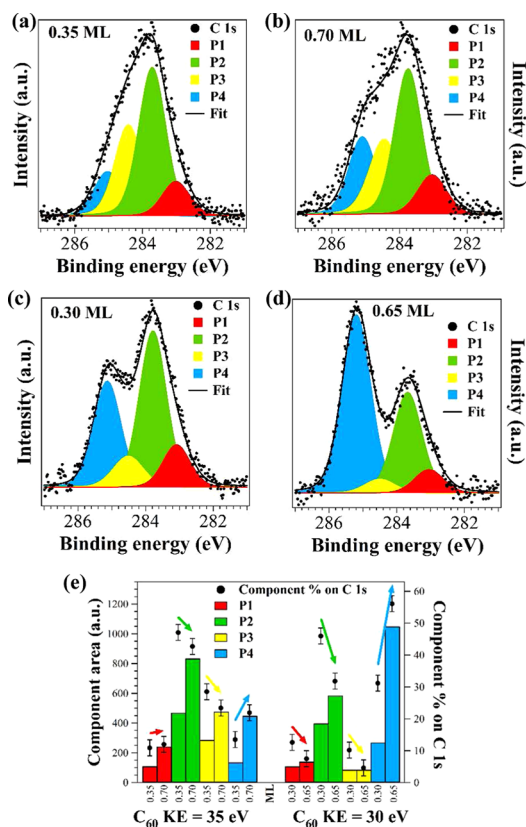


Figure 1. C 1s CLs (peaks normalized in height) of films grown at C_{60} KEs of 35 eV (a, 0.35 ML; b, 0.70 ML) and 30 eV (c, 0.30 ML; d, 0.65 ML). Components correspond to C in 3C-SiC (P1), SiC (P2), reacted C_{60} (P3), and physisorbed C_{60} (P4). (e) Component area and percentage of C 1s CL (variation followed by arrows).

35 eV, while at 30 eV the slight gain of the reacted species resulted in a strong enhancement of those physisorbed (Figure 1e).

Figure 2 shows the valence band (VB) spectra from UPS for C_{60} /Si films at 35 and 30 eV KE together with typical VB spectra of 3C-SiC, multilayer C_{60} , and Si(111) 7×7 . The 3C-SiC VB is characterized by two broad structures at about 4 and 9 eV, related to the p-like and sp-like molecular orbitals (MOs). The C_{60} spectrum has several distinct features, with peaks at 2.0 and 3.4

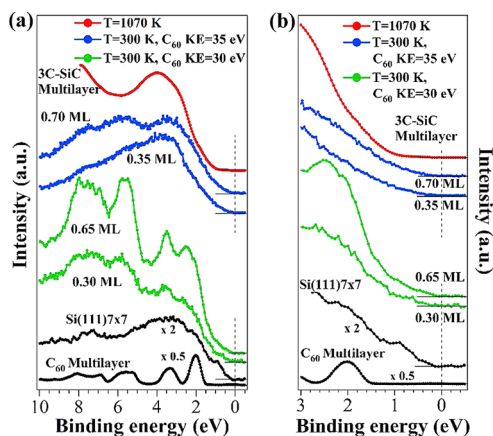


Figure 2. (a) VB spectra of films grown at C_{60} KEs of 35 and 30 eV and of substrate, C_{60} multilayer, and 3C-SiC films. (b) Zoomed-in view of the 0–3 eV BE range.

eV attributed to the highest occupied MO (HOMO) and to the so-called HOMO–1. The Si(111) 7×7 VB shows metallic character, with surface states at 0.2 and 0.9 eV (Figure 2b) and an overall intensity lower than those of C_{60} and SiC, causing the VB of C_{60} /Si films to be dominated mainly by the organic features.

The VBs of films at a C_{60} KE of 30 eV partially resemble those of organic multilayer structures with a +0.3 eV BE shift, in contrast to what was observed in MBE experiments at RT^{8,9,19} and $T = 670$ K.^{7,9} The C_{60} features are superimposed on an intense broad band whose intensity increases in going from 0.35 to 0.65 ML, indicating that this band is not representative of the Si(111) 7×7 substrate but instead is due to other carbon species. The Si surface states are depleted or absent, while two structures are present at 2.0 and 2.4 eV. In view of the observed BE shift, the 1.7 eV feature represents the former HOMO, while the 2.1 eV peak is assigned to C_{60} –Si chemical interactions at RT^{8,9,20} and $T \geq 570$ K.^{6,7,9} Therefore, these films are mainly due to cages that are physisorbed or show Si–C covalent bonds.

VBs of films at a C_{60} KE of 35 eV are characterized by higher intensity than for bare Si. A main structure is present at ~ 3.7 eV, while the Si(111) 7×7 surface states are absent. C_{60} MOs are detectable only in the 5–10 eV range at 0.70 ML. A similar VB has been found only for C_{60} /Si(111) 7×7 MBE experiments at $T \geq 1140$ K,^{6,7,9} when synthesis of 3C or amorphous SiC islands was achieved. The bands in the 4–10 eV range at 0.70 ML resemble those of C_{60} but with major broadening. A similar picture has been found only at ~ 1070 K and is evidence of cage breaking.^{6,7,9} Thus, SiC is present in both films, with broken cages at 0.70 ML.

In comparison with the MBE experiments, XPS and UPS analysis clearly highlights the role of the C_{60} KE in activating chemical/physical processes that otherwise would be forbidden under thermal equilibrium conditions at RT. Further confirmation was provided by Auger electron spectroscopy (AES) analysis²¹ (see the SI). The higher efficiency observed at 35 eV suggests the presence of a C_{60} KE threshold close to 30 eV, while the presence of crystalline 3C-SiC envisages a role of the precursor KE in also improving the structural order of the film. Low- T SiC growth by ionized-cluster beam deposition has been studied before, but the debate on this technique²² is still great and the 1 order of magnitude higher KE of the clusters leads to chemical and physical processes different from those typical of MBE and SuMBE.

Low-energy electron diffraction (LEED) analysis (50 eV) was performed on the four C_{60} submonolayer films. Si(111) 7×7 showed the well-known sharp diffraction pattern (Figure 3a). The two films at lower coverage exhibited LEED patterns with a diffuse background superimposed on the Si 7×7 features, while the 0.65 ML film at 30 eV showed only the Si 1×1 hexagonal spots. Similar results have been reported for RT MBE experiments,^{7,9,23} suggesting that the Si surface structure is hardly affected by the presence of the physisorbed C_{60} layer. The 0.70 ML film at 35 eV (Figure 3b) showed features of the 7×7 surface but also new hexagonal 1×1 extraspots, wider than the corresponding Si features. Subtracting the Si pattern from that of the 0.70 ML film (Figure 3c), we obtained black and white features corresponding to the Si(111) 7×7 pattern and the new 1×1 pattern. The lattice parameter of the new pattern is typical of a 3C-SiC(111) 1×1 structure.¹ In MBE experiments, LEED revealed an ordered carbide only at $T \geq 1300$ K,¹⁰ while at ~ 1100 K, SiC amorphous islands were formed.^{6,23} The observed superposition of the Si and SiC LEED patterns suggests the presence of 3C-SiC/Si islands with lateral dimensions of few tens

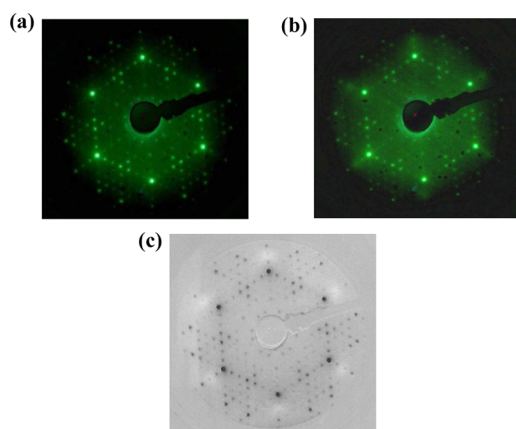


Figure 3. (a, b) LEED patterns (50 eV) for (a) the Si(111) 7×7 surface and (b) a 0.70 ML C_{60} /Si(111) 7×7 film formed at 35 eV KE, showing 3C-SiC 1×1 extraspots. (c) Subtraction of (a) from (b): dark areas belong to the 7×7 pattern and white spots to the new 3C-SiC 1×1 pattern.

of nanometers, given a typical 10–20 nm LEED electron coherence length.²⁴ As chemical analysis showed the presence of the carbide in its cubic phase in all of the films, the absence of the SiC pattern in the other three films suggests the presence of smaller 3C-SiC islands that LEED could not detect.

Ex-situ atomic force microscopy (AFM) and transmission electron microscopy (TEM) analyses were performed on the 0.65 ML film deposited at 30 eV KE, which was characterized by >50% physisorbed C_{60} and ~7.5% SiC from XPS analysis but the absence of 3C-SiC LEED pattern. The surface morphology (Figure 4a) shows the typical Si(111) terraces separated by

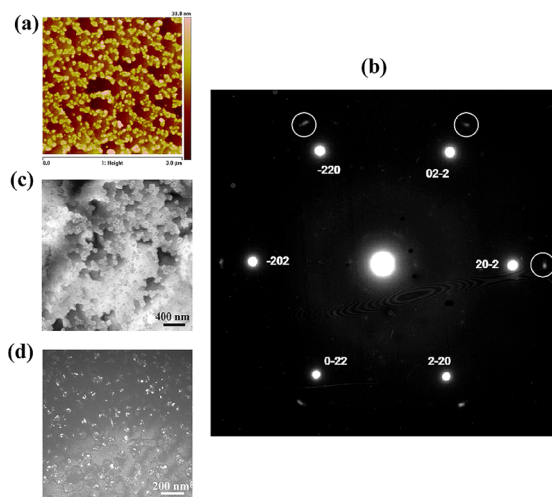


Figure 4. Microscopy analysis of the 0.65 ML C_{60} /Si(111) 7×7 film formed at 30 eV KE: (a) AFM image; (b) TEM diffraction pattern, with Si(111) bright spots and weak reflections from the 3C-SiC phase (circled spots); (c) bright-field TEM image; (d) dark-field TEM image.

multiple-atom steps. A high density of nanometer-sized island grains along the step edges, some tens of nanometers wide and ~10 nm high, are revealed on the terraces. In TEM analysis, the diffraction pattern in the (111) Si zone axis (Figure 4b) shows spots that can be unambiguously attributed to 3C-SiC epitaxially grown on Si(111) with lattice parameters of a completely relaxed structure. The bright-field TEM image (Figure 4c) shows terraces and nanograins mainly deposited along the step edges, in

accord with the AFM results. The dark-field TEM image (Figure 4d), which was taken using one of the (220) reflections of the 3C-SiC phase, indicates that the small grains at the Si terrace edges are nanometer-sized 3C-SiC islands. Their small size (~10 nm) is probably below the detectability of our LEED setup.

The low Si and C mobility at RT would suggest carbide formation of one or a very few layers on Si surface. Because of the lattice mismatch between 3C-SiC and Si(111), a single epitaxial carbide layer would be characterized by a strained structure, but we found ~10 nm high 3C-SiC islands with a completely relaxed lattice. This envisages the presence of non-negligible mobility of both C and Si atoms induced by C_{60} KE.

The differences in the chemical and structural properties of the films grown at the two C_{60} KEs confirmed the presence of a precursor energy threshold at ~30 eV for inducing several physical processes at the film surface at RT, first and foremost the cage breaking. This process triggers all further developments, so we modeled C_{60} -Si collisions using a number of computational tools at different levels of accuracy until we obtained a reliable description of the experimental findings.

Our first picture of the cage fragmentation was based on a mechanical effect: the collisional energy brings C_{60} to highly excited vibrational states, resulting in bond breaking. In this hypothesis, the collision would happen on a time scale of hundred of femtoseconds, making a description by ab initio MD feasible. While our DFT calculations found a rather strong chemisorption on the Si(111) surface, the C_{60} cage breaking occurred only for KE ≥ 300 eV, in agreement with previous calculations based on classical MD and tight-binding DFT.^{25,26} Details of these calculations can be found in the SI. Since this conclusion was strongly inconsistent with our experimental data, we considered the effect of electronic excitations as a possible reason for the cage rupture. In this hypothesis, the electrons cannot relax fast enough to the ground state relative to the instantaneous configuration of the nuclei and “lag behind”, creating an intense dipole moment responsible for the electronic excitation. Hence, the potential energy surface (PES) on which the nuclear motion occurs significantly changes, possibly allowing for cage breaking at lower KE.

To obtain a first indication of the importance of this effect, we used the Car–Parrinello (CP) approach to DFT-MD,²⁷ in which the electronic wave function is not optimized at each MD time step but instead is propagated by a Lagrangian, where the electrons have fictitious masses. This does not guarantee that the electronic wave function is exactly on the BO surface, but it is reasonably close. We intentionally increased the fictitious electronic mass to allow for a sizable deviation from the BO surface, effectively including in the wave function excitation that responds less promptly to the nuclear configuration changes. Within this approach, the minimum KE required to break the cage was 120 eV, which is much lower than that required by a classical impact mechanism, suggesting that electronic excitation might play an important role in this collision.

A full quantum treatment was unfeasible for our problem size, so we used the NA-MD approach, which approximates the dynamics by performing stochastic hops between adiabatic surfaces (ASs) constructed with excited states of the system. ASs were calculated using time-dependent DFT, while the probability of surface hopping among PESs was evaluated using the Landau–Zener theory.²⁸ The forces used in the MD simulation were calculated on the AS populated at the present MD step.

Unfortunately, the computational cost of simulating the C_{60} collision on Si(111) 7×7 was too high to obtain a result in a

reasonable time. Therefore, we considered a smaller yet realistic system with a three-layer Si(100) 2×1 slab that was equivalent to Si(111) 7×7 with regard to the C_{60} impact (Figure 5).

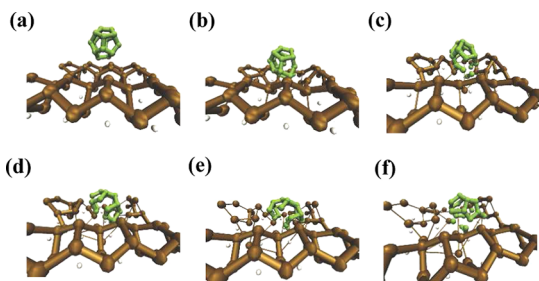


Figure 5. Snapshots of a trajectory for C_{20} impinging on Si(100) 2×1 at 11.3 eV from NA-MD calculations. Frames were taken every 22 fs.

Because of the smaller slab dimensions, we simulated the impact of a C_{20} molecule, whose main differences with C_{60} are the band gap (0.54 eV vs 1.64 eV) and the cohesive energy (-6.36 vs -7.15 eV/atom). The KE needed for the C_{20} fragmentation found by DFT exceeded 25 eV. To have the same energy per atom as in C_{60} , the initial velocities were kept constant. We included the six lowest-lying singlets and performed four simulations with initial KEs of 35, 22.6, 11.5, and 5.5 eV (corresponding to 105, 67.8, 34.5, and 16.5 eV in C_{60}) to find the KE threshold. Cage fragmentation occurred only in the first three cases and not in the last one. A C_{20} trajectory all the way from the initial condition to breaking is reported in Figure 5a–f.

Comparing the DFT and CP-DFT simulations for C_{60} and C_{20} , we infer that C_{60} cage breaking at energies as low as 0.6 eV/atom arises from changes in the force field felt by the nuclei due to the electronic excited state spawned upon impact with the surface. This effect, which cannot be captured by BO-MD simulations, provides grounds for all of the observed chemical/physical processes induced by the C_{60} KE on the Si surface.

In conclusion, we have synthesized nanocrystalline 3C-SiC on Si(111) at RT by SuMBE using a supersonic beam of C_{60} as the C precursor. Cage breaking and ordered carbide formation were observed, with the presence of 3C-SiC nanocrystals having a completely relaxed structure. A precursor KE threshold of ~ 30 eV was found. These results were perfectly supported by NA-DM studies developed for the C_{20} -Si(100) case under equivalent collisional conditions. Our study paves the way for the epitaxy of complete 3C-SiC layers in a SuMBE codeposition scheme with different supersonic beams of Si and C and the synthesis of SiC on substrates that cannot withstand high temperatures, such as plastic and polymers used in sensing and biomedicine.

■ ASSOCIATED CONTENT

📄 Supporting Information

Experimental and computational details. This material is available free of charge via the Internet at <http://pubs.acs.org>.

■ AUTHOR INFORMATION

Corresponding Author

roberto.verucchi@cnr.it; taioli@fbk.eu

Present Address

◆ Institut für Physik, Humboldt-Universität zu Berlin, 12489 Berlin, Germany.

Notes

The authors declare no competing financial interest.

■ ACKNOWLEDGMENTS

S.T. acknowledges financial support under the Marie Curie Action of the Seventh Framework Programme, The Trentino Program of Research, Training and Mobility, outgoing researcher and logistical support by University College London, and the Institute of Advanced Studies of the University of Bologna. This work made use of the HPC facilities of HECTOR (U.K.) and AURORA (Trento). R.V. is indebted to Claudio Corradi and Marco Pola for their technical assistance.

■ REFERENCES

- (1) *Properties of Silicon Carbide*; Harrys, G. L., Ed.; INSPEC: London, 1995.
- (2) Eddy, C. R., Jr.; Gaskill, D. K. *Science* **2009**, *324*, 1398.
- (3) Sadow, S. E. *Silicon Carbide Biotechnology*; Elsevier: Amsterdam, 2012.
- (4) Ramesh, P.; Itkis, M. E.; Bekyarova, E.; Wang, F.; Niyogi, S.; Chi, X.; Berger, C.; de Heer, W.; Haddon, R. C. *J. Am. Chem. Soc.* **2010**, *132*, 14429.
- (5) Masri, P. *Surf. Sci. Rep.* **2002**, *48*, 1.
- (6) De Seta, M.; Tomozeiu, N.; Sanvitto, D.; Evangelisti, F. *Surf. Sci.* **2000**, *460*, 203.
- (7) Sakamoto, K.; Kondo, D.; Ushimi, Y.; Harada, M.; Kimura, A.; Kakizaki, A.; Suto, S. *Phys. Rev. B* **1999**, *60*, 2579.
- (8) Sakamoto, K.; Harada, M.; Kondo, D.; Kimura, A.; Kakizaki, A.; Suto, S. *Phys. Rev. B* **1998**, *58*, 13951.
- (9) Cepek, C.; Schiavuta, P.; Sancrotti, M.; Pedio, M. *Phys. Rev. B* **1999**, *60*, 2068.
- (10) Sakamoto, K.; Susuki, T.; Harada, M.; Wakita, T.; Suto, S.; Kasuya, A. *Phys. Rev. B* **1998**, *57*, 9003.
- (11) Scoles, G. *Atomic and Molecular Beam Methods*; Oxford University Press: Oxford, U.K., 1988.
- (12) Iannotta, S. In *Cluster Beam Synthesis on Nano-Structured Materials*; Milani, P., Iannotta, S., Eds.; Springer: Berlin, 1999.
- (13) Aversa, L.; Verucchi, R.; Ciullo, G.; Ferrari, L.; Moras, P.; Pedio, M.; Pesci, A.; Iannotta, S. *Appl. Surf. Sci.* **2001**, *184*, 350.
- (14) Verucchi, R.; Aversa, L.; Ciullo, G.; Podestà, A.; Milani, P.; Iannotta, S. *Eur. Phys. J. B* **2002**, *26*, 509.
- (15) Zilani, M. A. K.; Xu, H.; Sun, Y. Y.; Wang, X.-S.; Wee, A. T. S. *Appl. Surf. Sci.* **2007**, *253*, 4554.
- (16) Mèlinon, P.; Kéghélian, P.; Perez, A.; Ray, C.; Lermé, J.; Pellarin, M.; Broyer, M.; Boudeulle, M.; Champagnon, B.; Rousset, J. L. *Phys. Rev. B* **1998**, *58*, 16481.
- (17) Liu, C.-C.; Lee, C.; Cheng, K.-L.; Cheng, H.-C.; Yew, T.-R. *Appl. Phys. Lett.* **1995**, *66*, 168.
- (18) Santoni, A.; Lancok, J.; Dhanak, V. R.; Loreti, S.; Miller, G.; Minarini, C. *Appl. Phys. A: Mater. Sci. Process.* **2005**, *81*, 991.
- (19) Moriarty, P.; Upward, M. D.; Dunn, A. W.; Ma, Y.-R.; Beton, P. H.; Teehan, D. *Phys. Rev. B* **1998**, *57*, 362.
- (20) Hou, J. G.; Yang, J.; Wang, H.; Li, Q.; Zeng, C.; Lin, H.; Bing, W.; Chen, D. M.; Zhu, Q. *Phys. Rev. Lett.* **1999**, *83*, 3001.
- (21) Taioli, S.; Simonucci, S.; Calliari, L.; Dapor, M. *Phys. Rep.* **2010**, *493*, 237.
- (22) Turner, D.; Shanks, H. *J. Appl. Phys.* **1991**, *70*, 5385.
- (23) Suto, S.; Sakamoto, K.; Wakita, T.; Hu, C.-W.; Kasuya, A. *Phys. Rev. B* **1997**, *56*, 7439.
- (24) Starke, U.; Pendry, J. B.; Heinz, K. *Prog. Surf. Sci.* **1996**, *52*, 53.
- (25) Galli, G.; Mauri, F. *Phys. Rev. Lett.* **1994**, *73*, 3471.
- (26) Hu, X.; Albe, K.; Averbach, R. S. *J. Appl. Phys.* **2000**, *88*, 49.
- (27) Car, R.; Parrinello, M. *Phys. Rev. Lett.* **1985**, *55*, 2471.
- (28) Landau, L. *Sov. Phys.* **1932**, *2*, 46.